Observation and Interpretation of Magnetic-Field-Line Reconnection and Tearing in a Theta Pinch

J. H. Irby, J. F. Drake, and Hans R. Griem
Department of Physics and Astronomy, University of Maryland, College Park, Maryland 20742
(Received 14 August 1978)

Measurements and calculations are presented of reconnection and tearing of magnetic fields in a theta pinch operated with initial bias and driving fields in opposite directions. Open magnetic field lines reconnect and form magnetic islands on time scales of the order of an Alfvén transit time across the plasma sheath. Implications of these results for plasma confinement are discussed.

Tearing instabilities are important in a wide range of physical systems ranging from the tail of the magnetosphere to laboratory fusion experiments. Variations in the radial light emission as a function of the distance along the axis of field-reversed θ pinches have previously been cited[1] as evidence for the existence of tearing modes in these elongated plasma rings. The magnetic structure in these experiments, however, could only be conjectured, making interpretation and comparison with theory extremely difficult. Magnetic probe measurements on the University of Maryland high-voltage fast theta pinch[2] (FTP) in the reversed-field configuration have revealed a diverse variety of magnetic tearing and reconnection processes, including the formation and coalescence of magnetic islands on time scales of the order of the Alfvén time across the field-reversal layer. In addition to being the first direct observation of tearing modes in neutral sheets, these magnetic field measurements demonstrate that reconnection of the inner and outer axial flux leads to the formation of closed magnetic surfaces, which should result in greatly improved electron energy confinement over an open-field system.[3]

Because of the absence of shear in the reversed-field pinch, the tearing-mode theory of Furth, Killeen, and Rosenbluth[4] (FKR) does not apply to this configuration. A theoretical investigation has therefore been carried out which demonstrates that the large growth rates of the experimentally observed tearing modes are a consequence of the ion Larmor radius ρ_i being comparable to the sheath thickness a.

The 1-m-long coil of the FTP[2] is 50 cm in diameter and surrounds a 46-cm-wide Pyrex vacuum vessel. The initial plasma is formed by switching into the coil a 60-kV, 83-kHz ringing discharge. This preheater is followed after 150 μsec by the firing of a crowbarred bias bank producing a uniform 200-G field when the main bank is fired 100 μsec later. The 600-nsec, 1-MA current pulse from the main bank is supplied to the coil by a Blumlein-type parallel-plate transmission line. All data presented here were taken in 6 mTorr D_2, with the bias field antiparallel to the 2500-G (maximum) main field. Other relevant parameters are an electron temperature of from 30 to 50 eV, radial and axial ion temperatures of 500 and 200 eV, and an initial electron density of about 2×10^{13} cm^{-3}.

To measure the axial magnetic field, B_z, we constructed a four-channel magnetic probe. The supporting boom of the probe was placed parallel to, but 17 cm from, the axis of the θ pinch. The 4-mm, two-turn probe tips were supported radially 17 cm from the boom so that they were at $r = 0$ when the probe was placed in the horizontal plane. The axial spacing of the probes was 15 cm. We could then map $B_z(r,z)$ by rotating the boom about its axis and translating the boom along z. In this manner B_z was measured at twelve axial (from the midplane at $z = 0$ to $z = 75$ cm) and eighteen radial positions. The final axial resolution was either 5 or 10 cm while the radial separation was between 1 and 1.5 cm. Five to ten shots were taken at each location. A high-order polynomial fit was used to smooth the raw data.

End-on photography along with magnetic-probe measurements has shown that both the implosion and post-implosion phases possess a high degree of azimuthal symmetry so that $\partial/\partial\theta \approx 0$. Also, the lack of significant axial currents implies $B_\theta \cong 0$. With these two assumptions

$$\vec{B}(r,z) = (\hat{i}_\theta/r)\times\nabla\psi(r,z), \tag{1}$$

where $\psi(r,z) \equiv rA_\theta(r,z)$ is the flux function. Integration of the z component of this equation gives

$$\psi(r,z=z_i) = \int_0^r B_z(r,z=z_i)r\,dr, \tag{2}$$

where by definition $\psi(0,z) = 0$ and z_i is the ith axial probe position. Because $\vec{B}\cdot\nabla\psi = 0$, a contour

plot of the flux is also a plot of the field lines. Thus, to map out the field lines it is necessary only to measure the axial component of the magnetic field.

There is considerable experimental evidence that the probes are producing reliable results. Both light and x-ray emission from the plasma showed little change with or without the probes present. Moreover, the movement of the observed magnetic islands has no correlation with probe position. The data were originally taken with 15-cm axial probe separation. Later, more data were taken to increase the axial resolution. The second set of flux plots was essentially identical to the first. In particular, even the small islands in Fig. 1(b) are insensitive to the data mesh.

Plots of the field lines are shown at four different times in Fig. 1. The dashed contour (separatrix) in each plot differentiates the closed- from the open-field lines. Figure 1(a) shows that the implosion progresses most rapidly in the end region ($z \sim 40$–50 cm) where the density is lowest, thus effectively pinching off the bulk of the plasma from the ends by magnetic reconnection. This produces a large island extending nearly the length of the coil region. Just 120 nsec later [Fig. 1(b)] this island has contracted axially and torn into smaller islands. The imploding field, which is peaked at the midplane of the column because of fringing in a finite solenoid, then tears the current at $z = 0$ [Fig. 1(c)], leading to the formation of two current rings [Fig. 1(d)] which remain stationary for about 1 μsec until the decay of the axial flux causes the plasma to expand radially. The existence of closed magnetic surfaces over times of order 1.5 μsec correlates well with previous observations[5] of good energy confinement over the same time interval.

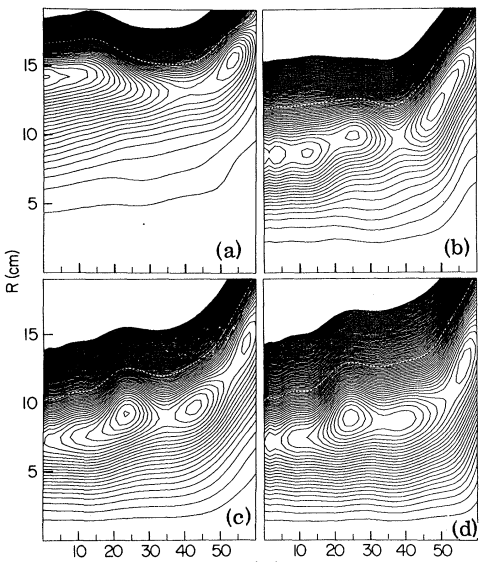

FIG. 1. Experimentally determined magnetic field lines shown at times $t = 0.40$, 0.52, 0.60, and 0.76 μsec. Each diagram maps one quadrant of the discharge, the axis of the maching being at $r = 0$ and the midplane at $z = 0$. The change in flux between adjacent field lines is $\Delta\psi = 2500$ G cm^2.

The magnetic islands shown in Fig. 1(b) grow from small amplitude during a time ~ 100 nsec and are apparently independent of boundaries and initial inhomogeneities.[6] We therefore interpret the formation of these islands as a tearing instability in contrast with the forced reconnection producing the large island shown in Fig. 1(a). Such an interpretation is consistent with the observation that $k_z a \lesssim 1$, k_z being the wave number of the islands, a necessary requirement for the tearing instability to be energetically favorable.[4]

In developing a theoretical model of this instability, it is essential to note the presence of the radial field B_r^0 in Fig. 1(a), which magnetizes the electrons essentially everywhere. Thus, calculations[7] based on a simple slab, reversed-field equilibrium [a current $J_y^0(x)$ produces a self-consistent $B_z^0(x) = B^0 \tanh(x/a)$ which reverses sign across $x = 0$], in which the electrons are unmagnetized in the vicinity of $B_z^0 = 0$, are not applicable to this experiment. However, the addition of a uniform component of the magnetic field B_x^0 normal to the current layer of this equilibrium leads to the configuration shown in Fig. 2(a), which models the essential features of the experiment. As long as $B_x^0 \ll B^0$, the field-reversed equilibrium and consequently J_y^0 and B_z^0 are locally unchanged by B_x^0.[8,9] Moreover, the variation of the equilibrium with z can be neglected as long as $k_z L_z \gg 1$, where L_z is the equilibrium scale length along z. In this limit, the magnetic field lines are simply parabolic in the region $|x| \ll a$ since the vector potential $A_y^0 \simeq B^0 x^2/2a + |B_x^0| z \equiv |B_x^0|(z + x^2/2\delta)$ is constant along $\vec{B}^0$. The electrons are magnetized everywhere if $\delta \gg (\rho_e a)^{1/2}$, $\rho_e = v_e/\Omega_e$ being the electron Larmor radius outside the sheath. The situation where $\rho_i \ll a$ is considered first for simplicity, although experimentally $\rho_i \simeq a$.

We consider magnetic perturbations

$$\tilde{\vec{B}} = \nabla \times [\tilde{A}_y(x,z)\hat{y}]$$

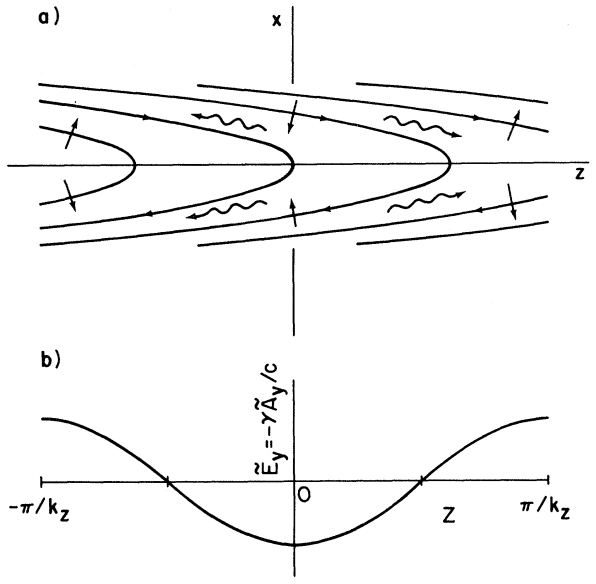

FIG. 2. (a) Equilibrium magnetic fields $\vec{B}^0$ used for the theoretical calculations. The perturbed field $\tilde{E}_y$ shown in (b) causes the electrons to move in the direction of the short arrows, leading to pressure imbalances which are relaxed by sound waves (wiggly arrows).

of the form shown in Fig. 1(b), where $\tilde{A}_y \propto \exp(i \times k_z z)$, with a corresponding electric perturbation

$$\tilde{\vec{E}} = -\gamma \tilde{\vec{A}}_y/c - \nabla\tilde{\varphi},$$

γ being the growth rate of the instability. Following standard procedure,[7] we can calculate $\tilde{A}_y$ in the vicinity of the magnetic field minimum around $x = 0$ and match this solution with the external magnetohydrodynamic (MHD) solution. In the region $|x| \ll a$, Maxwell's equation becomes

$$\partial^2 \tilde{A}_y/\partial x^2 = -(4\pi/c)(\tilde{J}_{ye} + \tilde{J}_{yi}), \tag{3}$$

where $\tilde{J}_{ye}$ and $\tilde{J}_{yi}$ are electron and ion currents in response to the induction field $-\gamma \tilde{A}_y/c$.

The electron response to the perturbed fields is calculated from the linearized fluid equations. The fluid description of the parallel electron motion is justified if the collision frequency ν_{ei} is larger than the bounce frequency in the magnetic well. The perturbed velocities parallel and perpendicular to $\vec{B}_0$ are

$$\tilde{v}_{\parallel e} = [m_e(\gamma + \nu_{ei})]^{-1} \frac{\partial(e\tilde{\varphi} - T_e \tilde{n}_e/n^0)}{\partial s}, \tag{4}$$

$$\tilde{\vec{v}}_{\perp e} = \left[\frac{e\gamma \tilde{\vec{A}}_y}{c} + \nabla_\perp\left(e\tilde{\varphi} - \frac{T_e \tilde{n}_e}{n^0}\right)\right] \times \frac{\vec{\Omega}_e}{\Omega_e^2 m_e}, \tag{5}$$

where $\partial/\partial s = (\vec{B}^0/|\vec{B}^0|)\cdot\nabla$. The continuity equation,

$$\gamma \tilde{n}_e + n_0 \nabla\cdot \tilde{\vec{v}}_{\perp e} + n_0 B^0 \frac{\partial(\tilde{v}_{\parallel e}/B^0)}{\partial s} = 0, \tag{6}$$

completes the description of the electrons. When $\gamma \gg \Omega_{ix}$, Ω_{ix} being the ion gyrofrequency in $B_x{}^0$, the ions are unaffected by $B_x{}^0$. The ions are therefore unmagnetized in a region $|x| < (\rho_i a)^{1/2}$, as in the standard reversed-field sheet.[7] Within this region the ions respond adiabatically to $\tilde{\varphi}$,

$$\tilde{n}_i \simeq -n^0 e\tilde{\varphi}/T_i \simeq \tilde{n}_e, \tag{7}$$

where charge neutrality has been invoked. Equations (4)–(7) are combined into a single equation for $\tilde{n}_e$ as follows:

$$\left(1 - S^2 B^0 \frac{\partial}{\partial s}\frac{1}{B^0}\frac{\partial}{\partial s}\right)\tilde{n}_e = \frac{n^0 e}{m_e c}\nabla\cdot\frac{\tilde{\vec{A}}_y \times \vec{\Omega}_e}{\Omega_e{}^2}, \tag{8}$$

where $S^2 = V_{es}{}^2/\gamma(\gamma + \nu_{ei})$ and $V_{es} = [(T_e + T_i)/m_e]^{1/2}$ is the electron sound velocity. The operator on the left-hand side of Eq. (8) represents sound-wave propagation in this geometry, the electrons and ions having reversed roles by virtue of the adiabatic ion response and fluid electron response to $\tilde{\varphi}$. The electron dynamics can be understood from Fig. 2. The periodic induction field $\tilde{\vec{E}}_y$ causes the electrons to $\tilde{\vec{E}}\times\vec{B}$ drift in the direction of the small arrows. This flow has nonzero divergence and therefore modulates the electron density along z. The resulting pressure imbalance parallel to $\vec{B}^0$ produces outgoing compression and rarefaction waves (wiggly arrows), strongly reducing $\tilde{n}_e$. The coupling to the sound wave is weak in the collisionless limit.[9] Inversion of the operator in the left-hand side of Eq. (8) yields the residual electron density perturbation,

$$\tilde{n}_e \simeq -n_0(R_m/|B_x{}^0|S)(\tfrac{1}{2}ik_z\delta\pi)^{1/2} \times [\tilde{A}_y(z + x^2/2\delta)]\exp(-|s|/S), \tag{9}$$

which is approximately constant along $\vec{B}^0$ out to a distance S. The quantity R_m is the mirror ratio along a given field line ($R_m = B^0/|B_x{}^0|$ in a system which is homogeneous along z). This density perturbation produces a diamagnetic current along $\hat{y}$, which from Eq. (5) is

$$\tilde{J}_{ey} = -(T_e + T_i)ik_z c\tilde{n}_e/|B_x{}^0|. \tag{10}$$

This current oscillates rapidly with x for $|x| > (\delta/k_z)^{1/2}$ and, consequently, only the contribution from $|x| < (\delta/k_z)^{1/2}$ is important.

The ion current is large in the unmagnetized region $|x| < (\rho_i a)^{1/2}$ and has been previously cal-

culated as[7]

$$\tilde{J}_{yi} = -(\omega_{pi}^2/4\pi c)(\pi^{1/2}\gamma/k_z v_i)\tilde{A}_y, \quad |x| < (\rho_i a)^{1/2}, \qquad (11)$$

where $(\omega_{pi}^2/c^2)\tilde{A}_y$ is the collisionless response and $\gamma/k_z v_i < 1$ arises because only ions with velocity $v_z < \gamma/k_z$ receive a dc acceleration. The ion and electron currents produce a discontinuity in the slope of $\tilde{A}_y$ across $x = 0$, which is calculated by integrating Eq. (3). The dispersion relation of the tearing mode then follows by matching with the corresponding discontinuity $\Delta' = [\partial\tilde{A}_y/\partial x]_{0-}^{0+}/\tilde{A}_y(0)$ of the outer MHD solution,

$$g\left(\frac{\gamma}{\Omega_i}\right)\left(\frac{a}{\rho_i}\right)^{5/2} + R_m\left(\frac{a^2}{\delta V_{es}}\right)[\gamma(\gamma+\nu_{ei})]^{1/2} = \frac{2\Delta'}{k_z\pi}, \qquad (12)$$

where $g^{-1} = \pi^{1/2}k_z^2a^2(T_e+T_i)/T_i$. The first and second terms in Eq. (12) arise from the ions and electrons, respectively.

The growth rate resulting from (12) is sensitive to the quantity ρ_i/a. When $\rho_i/a \ll 1$, the ion contribution dominates and $\gamma/\Omega_i \lesssim (\rho_i/a)^{5/2}$. The growth rate increases rapidly with ρ_i/a until the electron term in (12) becomes important. In the present experiment $\rho_i > a$ and the ions are confined by their electrostatic attraction with the electrons rather than by the magnetic field. The calculation[10] of the growth rate of the tearing mode is virtually unchanged, however, except that the ion current $\tilde{J}_{yi}$ can be neglected in Eq. (3). The growth rate for $\rho_i > a$ is simply obtained by neglecting the ion contribution in Eq. (12). For the experimental parameters ($\rho_i \simeq 1.5a \approx 2.5$ cm, $B^0 \approx 20B_r^0 \simeq 1$ kG, $R_m \approx 4$, and $k_z a \approx 1$), $\gamma \approx 0.5\times 10^7$/sec, which is in reasonable agreement with experimental observations. Such large growth rates ($\gamma \approx \Omega_i$) are only possible when $\rho_i \gtrsim a$.

Of substantial theoretical and experimental interest is the nonlinear evolution of this tearing mode. Preliminary calculations[10] indicate that the growth of the instability is strongly reduced as closed magnetic islands are formed when $\tilde{B}_x \approx B_x^0$. This saturation amplitude is consistent with our experimental observations and may explain the apparent absence of this mode in streak photographs of larger-aspect-ratio, field-reversed pinches.[3]

We are happy to acknowledge many helpful conversations with A. Allen, Y. G. Chen, F. V. Coroniti, Y. C. Lee, C. S. Liu, and R. Pellat, and the technical assistance of T. Torres and W. Crowe. This research was supported by the U. S. Department of Energy.

[1]H. A. B. Bodin, Nucl. Fusion 3, 215 (1963).

[2]A. W. DeSilva *et al.*, in *Plasma Physics and Controlled Nuclear Fusion Research* (International Atomic Energy Agency, Vienna, 1969), Vol. I, p. 143.

[3]A. Aberhagen and W. Grossman, Z. Phys. 248, 130 (1971); R. K. Linford, D. A. Platts, E. G. Sherwood, and K. S. Thomas, Bull. Am. Phys. Soc. 22, 1191 (1977).

[4]H. P. Furth, J. Killeen, and M. N. Rosenbluth, Phys. Fluids 6, 459 (1963); see also J. F. Drake and Y. C. Lee [Phys. Fluids 20, 1341 (1977)] for a more physical discussion and extensions to higher temperature regimes.

[5]Roger A. Hess and Hans R. Griem, Phys. Fluids 18, 1056 (1975).

[6]D. F. Düchs, R. H. Dixon, and R. C. Elton, Phys. Fluids 17, 124 (1974).

[7]G. Laval, R. Pellat, and M. Vuillemin, in *Plasma Physics and Controlled Nuclear Fusion* (International Atomic Energy Agency, Vienna, 1965), Vol. II, p. 259.

[8]A. A. Galeev and L. M. Zelenyi, Zh. Eksp. Teor. Fiz. 70, 2133 (1976) [Sov. Phys. JETP 43, 1113 (1976)].

[9]B. Lemberge and R. Pellat, unpublished.

[10]J. F. Drake and C. S. Liu, to be published.